RSC Advances

PAPER

View Article Online
View Journal | View Issue

Check for updates

Cite this: *RSC Adv.*, 2024, **14**, 32001

Chemical induces microstructural transformation of pulp fibre to colloidal cellulose for sustainable plant protection†

Apichat Phengdaam, *[a] Jiranat Chaiyosburana,[b] Wichayut Hianchasri,[c] Nutthaphol Khupsathianwong, [d] Nattapon Uthaipan[e] and Sanong Ekgasit*[c]

Cellulose, an environmentally friendly material, is abundantly available in Thailand as pulp and has significant potential for use in sustainable plant protection; however, the raw material is not directly suitable for such applications. To address this, colloidal cellulose with high water dispersibility was synthesised by treating Eucalyptus pulp with sulphuric acid (H_2SO_4). The optimised conditions involved a 24 hour treatment, producing colloidal cellulose with an average particle size of 0.57 ± 0.03 μm, the smallest size achieved. The cellulose morphology, consisting of submicron and nanoscale fragments and particles, was confirmed by transmission electron microscopy, field-emission scanning electron microscopy, and dynamic light scattering analyses. This microstructural transformation, driven by H_2SO_4-induced gelatinization and regeneration, led to decreased crystallinity, as observed in X-ray diffraction patterns and infrared spectra. The formation of colloidal cellulose as a film with adhesive properties on complex plant surfaces is facilitated by hydrogen bonding and hornification mechanisms. Additionally, colloidal cellulose demonstrated high compatibility with cuprous oxide, which was used as a model agricultural protective agent, showing a reduction of over 99% in *E. coli* and *S. aureus* abundance, highlighting the potential of colloidal cellulose as a sustainable coating agent or adjuvant in agricultural protection strategies.

Received 13th September 2024
Accepted 3rd October 2024

DOI: 10.1039/d4ra06600f

rsc.li/rsc-advances

Open Access Article. Published on 09 October 2024. Downloaded on 4/26/2026 2:10:51 AM.
This article is licensed under a Creative Commons Attribution-NonCommercial 3.0 Unported Licence.

1. Introduction

Cellulose, an abundant and eco-friendly biopolymer, is receiving increasing research attention due to the growing emphasis on sustainability across many sectors. Sourced from industrial plants such as eucalyptus,[1] pine trees,[2] and pineapple leaves,[3] cellulose is a key material used in a range of industries. Its widespread application, often involving conversion into high-purity pulp, is driven by its low toxicity, broad availability, and compatibility with diverse material surfaces.[4] In Thailand alone, the pulp industry consumes over 3.8 million tons of cellulose annually, supporting multiple paper industries.[5] Its versatility has led to the development of diverse cellulose-based products ranging from food packaging[6] and biodegradable films to energy storage devices[7] and medical applications;[8] thus, high-purity cellulose is a sustainable material with a widespread variety of industrial and healthcare applications.[9,10]

There is an increasing focus on reducing synthetic chemical use, such as fertilizers and pesticides, in modern agriculture to produce high-quality, safe, and environmentally friendly products, a practice known as organic farming.[11] A key strategy in organic farming is the use of natural substances like cellulose, a biodegradable material with significant potential. Cellulose has a variety of agricultural applications, including fungicides, fruit coatings, and soil moisture retention agents.[4,12] The effective management and renewability of natural resources have been demonstrated through cellulose applications.[13,14] These examples promote sustainable approaches aligned with the United Nations' Sustainable Development Goal (SDG) 12: "Responsible Consumption and Production".[15] As a natural, environmentally friendly substance, cellulose represents a sustainable option with diverse uses, thus promoting responsible agricultural practices in line with the SDG principles.

Cellulose consists of glucose subunits linked by β-1,4-glycosidic bonds, in contrast to the α-1,4-glycosidic bonds found in starch.[4] Hydrolysis of these bonds produces various forms of cellulose, including nanofibers, nanocrystals, amorphous cellulose, and microcrystalline cellulose.[10] The morphology and properties of these forms can be controlled by using different

[a]*Division of Physical Science, Faculty of Science, Prince of Songkla University, Hat Yai, Songkhla 90110, Thailand. E-mail: apichat.p@psu.ac.th*

[b]*NIST International School, Klongtoey-nua, Wattana, Bangkok 10110, Thailand*

[c]*Sensor Research Unit, Department of Chemistry, Faculty of Science, Chulalongkorn University, Bangkok 10330, Thailand. E-mail: sanong.e@chula.ac.th*

[d]*Technopreneurship and Innovation Management Program, Graduate School, Chulalongkorn University, Bangkok 10330, Thailand*

[e]*Rubber Engineering and Technology Program, Department of Specialized Engineering, Faculty of Engineering, Prince of Songkla University, Hat Yai, Songkhla 90110, Thailand*

† Electronic supplementary information (ESI) available: Size distribution, FE-SEM images, TEM images and TGA profiles of colloidal cellulose. See DOI: https://doi.org/10.1039/d4ra06600f

© 2024 The Author(s). Published by the Royal Society of Chemistry

Open Access Article. Published on 09 October 2024. Downloaded on 4/26/2026 2:10:51 AM. This article is licensed under a Creative Commons Attribution-NonCommercial 3.0 Unported Licence.

acids, such as, hydrochloric acid, phosphoric acid and sulphuric acid (H_2SO_4).[16] Among these, H_2SO_4 is particularly effective as it rapidly hydrolyses the amorphous regions of cellulose while preserving crystalline regions, which are decorated with sulphate groups due to the action of H_2SO_4, resulting in a stable water suspension.[17,18] The choice of acid in cellulose processing significantly influences the particle size of the product, ultimately affecting its water dispersibility and suitability for different agricultural applications. Processed cellulose exhibits excellent water dispersibility and colloidal stability,[19] thus making pulp an ideal raw material for colloidal cellulose synthesis.

Pulp, a fibrous lignocellulosic material, serves as the primary raw material in the manufacture of paper and other industrial paper products due to its high cellulose content, typically exceeding 70%.[20] Pulp fibres typically range from 1 to 5 mm in length and exhibit branched or aggregated structures.[21] Due to this network structure, pulp fibre cannot be dispersed in water. Water-soluble agents are more suitable for agricultural applications; therefore, reducing the pulp fibre size to the colloidal scale is essential for achieving a solution with stable dispersion. To achieve this, H_2SO_4 was used as an acidic treatment to cleave the β-1,4 glycosidic bonds, which form the main backbone of the cellulose fibres.

In this study, pulp with a high cellulose content was effectively converted from a long fibre structure into smaller fragments through sulfuric acid (H_2SO_4) treatment. This transformation was confirmed through morphology and particle size analyses conducted using field-emission scanning electron microscopy (FE-SEM), dynamic light scattering (DLS) techniques, and transmission electron microscopy (TEM). The crystallinity and molecular structure of the modified cellulose were further characterised using X-ray diffraction (XRD) and infrared spectroscopy (IR). The resulting cellulose particles exhibited excellent water dispersibility and long-term colloidal stability. These particles were readily transformed into films with good adhesion to complex plant surfaces. Importantly, the modified cellulose did not interfere with the activity of disinfectants or antimicrobial agents, thus making it an ideal carrier or adhesion enhancer for organic or non-toxic agriculture. This application is consistent with SDGs by promoting the sustainable production of safe, environmentally friendly food.

2. Materials and methods

2.1. Chemicals and materials

The eucalyptus pulp used in this study was sourced from Phoenix Pulp and Paper Plc Ltd (Thailand). The H_2SO_4 (97 wt%) was obtained from Sigma-Aldrich and used without further purification. Dialysis tubing, with a 14 000 Da molecular weight cutoff, was purchased from Innovating Science. All the chemicals were of analytical grade and used as received. Deionised (DI) water was used as the solvent throughout the study.

2.2. Synthesis of colloidal cellulose

The colloidal cellulose was synthesised using an acidic treatment process adapted from previous research.[22] Initially, approximately 5 g of pulp sheet was cut into 1 cm^2 pieces and soaked in 40 mL of 30% v/v H_2SO_4 for varying durations (6, 12, 24, and 48 hours). During this step, the pulp dispersed easily in the medium. The pre-treated pulp was then mixed with 40 mL of 80% v/v H_2SO_4 and stirred at 750 rpm. This strong acidic treatment induced a vivid yellow colour, indicative of the cleavage of cellulose derivatives and glucose molecules.[23] After 1.5 hours of stirring, the pulp transitioned into a cellulose gel, to which 415 mL of DI water was progressively added while mixing at 1500 rpm using a homogenizer for 5 minutes. The resulting opaque yellowish-white solution, indicating colloidal dispersion, underwent dialysis for 7 days to adjust the pH to 5–6. This process ultimately yielded an opaque white colloidal solution.

2.3. Characterization of colloidal cellulose

The pulp samples subjected to acidic treatment, along with the untreated pulp, were analysed using various techniques to assess their dimensions, morphology, and crystalline structure. The FE-SEM (Quanta FEG 250, FEI), DLS (Mastersizer 3000, Malvern) and TEM (JEM-2100 TEM, JEOL) techniques were employed to examine the samples' dimensions and morphology. XRD patterns were collected using an X-ray diffractometer (SmartLab, Rigaku) operated at 40 kV and 40 mA with CuKα radiation. Attenuated total reflection-Fourier transform infrared (ATR-FTIR) spectroscopy (Nicolet iS5, Thermo Scientific) with a diamond probe was used to obtain molecular bonding information across a wavenumber range of 400 to 4000 cm^{-1}. The adhesion properties were evaluated *via* a lap shear test on a universal testing machine (EX800Plus, Lloyd) with a 1 kN load at a crosshead speed of 10 mm min^{-1}. The interfacial phenomena were studied using a contact angle goniometer (Model 200-F1, Ramé-Hart Instrument), and the temperature profile was analysed using a thermogravimetric analyser (PYRIS-1 TGA, Shelton) under a nitrogen atmosphere.

2.4. Antimicrobial efficacy

The antimicrobial efficacy of an agricultural protective agent, with and without colloidal cellulose, was evaluated using a modified BSEN 1276:2019 protocol[24] provided by the Department of Microbiology, Chulalongkorn University, Thailand. Cuprous oxide (Cu_2O) was chosen as the model agricultural protective agent to assess the influence of colloidal cellulose on antimicrobial activity. In this test, 5 mL/5 mL inoculum/sample was initially incubated in darkness at 37 °C with a humidity of 90% for 15 minutes. The antimicrobial effectiveness was tested against *Escherichia coli* (*E. coli*) and *Staphylococcus aureus* (*S. aureus*), and the percentage reduction was calculated based on the viable bacterial count before and after treatment.

3. Results and discussion

3.1. Influence of acidic treatment

In this work, two highly effective cellulose hydrolysis steps were applied using two different concentrations of H_2SO_4. The first step (pre-treatment) recrystallizes the cellulose while the second

 © 2024 The Author(s). Published by the Royal Society of Chemistry

Open Access Article. Published on 09 October 2024. Downloaded on 4/26/2026 2:10:51 AM.
This article is licensed under a Creative Commons Attribution-NonCommercial 3.0 Unported Licence.

step (post-hydrolysis) converts the amorphous cellulose to glucose.[25] This process not only reduces the length of cellulose chains into smaller fragments with water-soluble molecules but also induces gelatinization and regeneration, thus influencing the crystallinity and size of the resulting cellulose structures.[22] The efficiency of cleaving the cellulose units depended on the H_2SO_4 concentration and incubation time.[26]

To investigate the impact of acidic treatment on cellulose morphology, raw pulp was treated with a high concentration of H_2SO_4 for 6, 12, 24, and 48 hours. The high acid concentration was chosen to minimize the incubation time. FE-SEM was employed to evaluate the size and morphological changes in the pulp before and after acidic treatment, as shown in Fig. 1. The untreated pulp (Fig. 1A) displayed long, branched fibres up to several micrometres in length, with an estimated diameter of approximately 10 μm. Upon visual observation, the fibre rapidly separated from the dispersion after mixing with water. Following treatment with H_2SO_4 for 6–24 hours (Fig. 1B–D), the fibres were fragmented from long to short submillimetre lengths, with packing of small particles observed at the bottom of the specimen. Following the drying process, a white thin film of synthesised cellulose was observed, while the dispersion remained opaque white, indicating the presence of colloidal-sized particles.

To quantify this effect, DLS was applied to measure the fibre size distribution (ESI, Fig. S1†). The average size decreased from 3.94 ± 0.64 μm at 6 hours to 1.83 ± 0.25 μm at 12 hours and further to 0.57 ± 0.03 μm at 24 hours. Notably, at 48 hours, two distinct fibre size distributions were observed, with an average of 0.64 ± 0.07 μm and 5.47 ± 0.07 μm, likely caused by the aggregation of smaller fibres to reduce surface energy for self-stabilization (ESI, Fig. S2†).[27] The initial observations suggested that a 24 hour acidic treatment produced the smallest cellulose short fibres; however, FE-SEM analysis revealed the presence of larger fibres (100 μm in fibre length, approximately) inconsistent with the DLS data. To clarify this discrepancy, TEM was used, which confirmed the presence of nanocellulose after 24 hours of acidic treatment (ESI, Fig. S3†). Consequently, the 24 hour treatment duration was selected for subsequent experiments.

3.2. Microstructural detail of colloidal cellulose

The submicron-scale colloidal cellulose obtained from the previous section was used for a detailed investigation of its physical properties and molecular characteristics. During the acidic treatment, not only did the particle size of the long-chain cellulose fibres decrease but the crystallinity of the cellulose also likely changed. In plant applications, the crystallinity of cellulose is a key property that influences this material's mechanical strength, water affinity, and reactivity to chemical agents.[28] Thus, the crystallinity of the colloidal cellulose was analysed and compared with that of the original material. The XRD patterns of both samples (Fig. 2) show a maximum peak intensity corresponding to the (002) facet of crystalline cellulose. The crystallinity index (CI), representing the percentage of crystalline cellulose, was calculated using eqn (1).[29,30]

$$\mathrm{CI} = \frac{(I_{002} - I_{\mathrm{am}})}{I_{002}} \times 100 \quad (1)$$

where I_{002} and I_{am} represent the XRD intensities at 2θ angles of 22.6° and 18.6°, corresponding to the (002) facets of crystalline and amorphous cellulose, respectively. Normally, the XRD peaks of the treated sample are broader than those of the original pulp, indicating a reduction in crystalline content following treatment.[31] The CI of the original material was calculated as 86%, whereas the colloidal cellulose exhibited a lower CI of 68%. This observed 20% decrease in crystallinity suggests that the high-crystallinity cellulose in the pulp source was transformed into an amorphous or non-crystalline form during treatment.

Additionally, IR spectroscopy was applied to compare the molecular structures of the original and acid-treated cellulose (Fig. 3). The results revealed that most band assignments were consistent between the two samples, including the C–H rocking vibration at 890 cm^{-1}, the C–C, C–OH, C–H ring, and side group vibrations at 1030 cm^{-1}, C–O–C stretching of the β-1,4-glycosidic linkages at 1160 cm^{-1}, symmetric CH_2 bending vibration (crystallinity band) at 1435 cm^{-1}, O–H bending of absorbed water at 1650 cm^{-1}, the C–H stretching vibration at 2890 cm^{-1}, and the O–H stretching vibration at 3330 cm^{-1}.[32,33] These

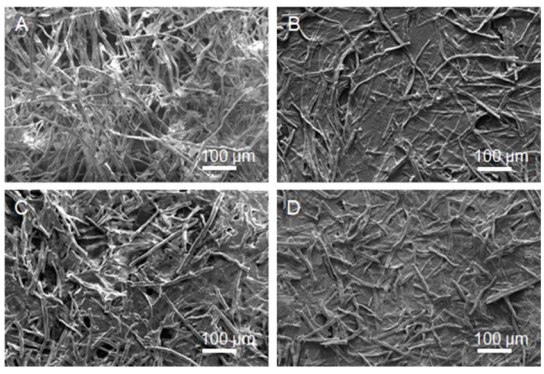

Fig. 1 FE-SEM images showing pulp fibre structure (A) before acidic treatment and the transformed structures after acidic treatment at 6, 12, and 24 hours (B, C, and D, respectively).

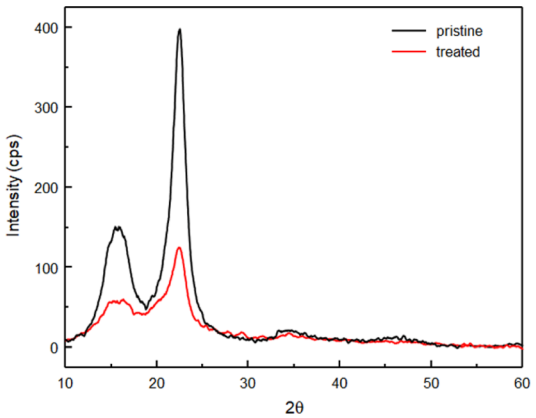

Fig. 2 XRD patterns of original pulp fibre (pristine) and colloidal cellulose (treated).

Open Access Article. Published on 09 October 2024. Downloaded on 4/26/2026 2:10:51 AM.
This article is licensed under a Creative Commons Attribution-NonCommercial 3.0 Unported Licence.

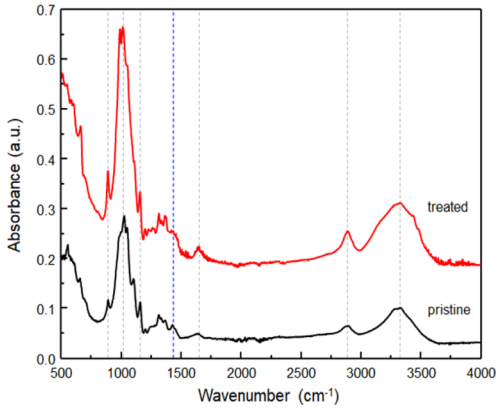

Fig. 3 IR spectra of original pulp fibre (pristine) and colloidal cellulose (treated).

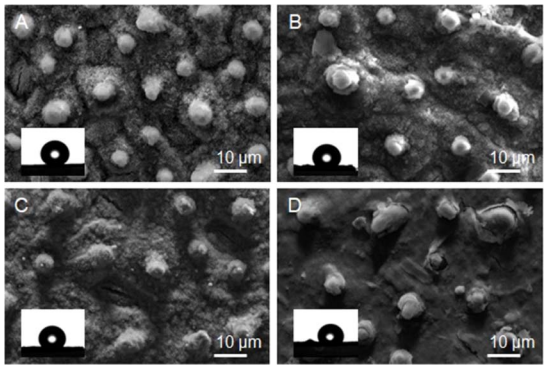

Fig. 4 FE-SEM images of lotus-leaf surface sprayed with 1.5% w/v colloidal cellulose for (A) 0, (B) 10, (C) 20 and 30 (D) seconds, with inset digital images showing the DI water contact angle for each configuration.

consistent band assignments confirm that the molecular structure of the cellulose remained largely intact during the treatment process, with no significant residual impurities post-purification (grey dashed line, Fig. 3). Notably, the O–H group, responsible for the water-dispersibility of the colloidal cellulose, was still present.[34] However, the crystallinity band at 1435 cm^{-1} (blue dashed line, Fig. 3) was less intense in the colloidal cellulose compared to the original pulp, indicating that the acid treatment process reduced the crystallinity of the cellulose, consistent with the observations from XRD data.

Overall, our study not only achieved colloidal-sized cellulose particles but also significantly decreased the crystallinity of the cellulose compared to the original pulp fibre. As previously reported, the amorphous form of cellulose is characterised by enhanced hydrophilicity, reactivity, and enzymatic digestibility compared to the more thermodynamically stable crystalline cellulose.[12,35] Therefore, colloidal cellulose with non-crystalline parts may improve the potential of this material for agricultural applications, which we explore further in Section 3.4.

3.3. The assembly of colloidal cellulose

Under drying conditions, the colloidal cellulose self-assembled into a film, as confirmed by visual inspection and FE-SEM imaging (Fig. 1), indicating its potential application as a coating agent or adjuvant for agricultural protective agents. To demonstrate its excellent surface adhesion properties, colloidal cellulose was applied to complex plant structures. The lotus leaf, known for its superhydrophobic characteristics, was chosen as the test substrate. FE-SEM images revealed the intricate surface architecture of the lotus leaf (Fig. 4A), including papillae, wax clusters, and wax tubules, all of which contribute to its remarkable water repellence.[36] The water contact angle on this surface measured 152°, confirming its superhydrophobicity (inserted photo, Fig. 4A). A 1.5% w/v colloidal cellulose solution was then sprayed onto the lotus leaf for 10 seconds (Fig. 4B), 20 seconds (Fig. 4C), and 30 seconds (Fig. 4D). Notably, concentrations above 1.5% w/v caused the spray head to become blocked; thus, the maximum possible concentration of 1.5% w/v was used here.

Microscopic analysis revealed that the colloidal cellulose assembled into a film layer, with more complete coverage achieved with longer spray durations. The formation of this film altered the lotus leaf's wettability, as evidenced by the decrease in water contact angles to 132°, 130°, and 120° after spray times of 10, 20, and 30 seconds (inserted photo, Fig. 4B–D), respectively. These results demonstrate that colloidal cellulose can be effectively applied *via* spraying, with the potential to fully coat hierarchical structures and plant leaf surfaces.

To investigate the adhesive properties of the obtained colloidal cellulose, lap shear tests were conducted on wood using colloidal cellulose of concentrations ranging from 1.5% to 3.0% w/v. The test results revealed wood–adhesive interfacial failures, as classified according to the ASTM D5573 standard, which identifies six primary failure modes.[37] All the samples exhibited adhesive failure with opaque white film remaining on the wood surface, indicating varying levels of adhesive strength.[38,39] The average shear strength (MPa) and standard deviation were calculated from three specimens per condition. As shown in Fig. 5, the shear stress *versus* strain percentage plot indicates a maximum shear stress of 0.14 ± 0.01 MPa for the highest cellulose concentration. A 30% reduction in shear stress was recorded for the samples with cellulose concentrations of 2.0% and 1.5% w/v, both yielding values of 0.10 ± 0.01 MPa. The stress–strain curves suggest that colloidal cellulose exhibits weak adhesive properties, with a pronounced tendency towards brittleness.[40,41] At a concentration of 1.0% w/v, the colloidal cellulose failed to adhere to the wood in the lap shear test, demonstrating lower adhesion than carboxymethyl cellulose applied at a similar concentration.[42]

The brittleness implied by the shear stress–strain curve suggests that the material's high cohesive strength leads to cracking.[43] Furthermore, adhesive failure likely occurs due to mechanical interlocking at the interface without chemical bonding.[44] This failure type and trend from lap shear tests indicate that colloidal cellulose may self-accumulate rather than form bonds with other substrates. This hypothesis is plausible, given that both crystalline and amorphous cellulose structures primarily exhibit cohesive forces from hydrogen

© 2024 The Author(s). Published by the Royal Society of Chemistry

Open Access Article. Published on 09 October 2024. Downloaded on 4/26/2026 2:10:51 AM.
This article is licensed under a Creative Commons Attribution-NonCommercial 3.0 Unported Licence.

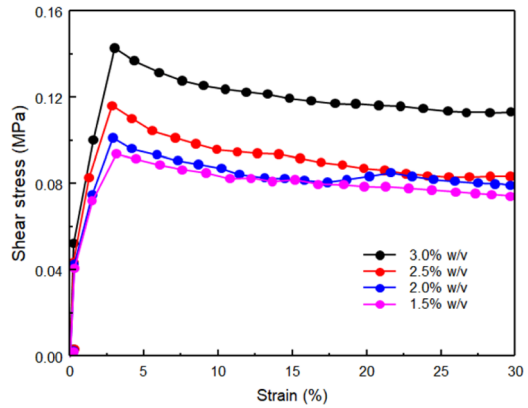

Fig. 5 Shear stress–strain curves of colloidal cellulose during lap shear testing with colloidal cellulose concentrations ranging from 1.5 to 3.0% w/v.

bonding, along with significant dispersion forces and electrostatic interactions.[45] The self-forming nature of cellulose, along with its ability to connect surface particles, is reliant on hydrogen bonding; however, the weaker adhesive properties of colloidal cellulose compared to cellulose derivatives may result from reduced hydrogen bonding.[46] Therefore, the hydrogen bonding of colloidal cellulose compared to pulp fibre should be investigated in further detail in future research.

Hydrogen bonding plays a key role in the interactions between cellulose chains, significantly influencing their morphological transformation. The IR spectra shown in Fig. 3 highlight the primary vibrational mode of the OH group at 3330 cm^{-1}. To explain the other hydrogen bonding activity, the band assignments within the 3000–3700 cm^{-1} range are densely concentrated, corresponding to the vibrational activity of the O–H bond, which is indicative of cellulose.[47] To further analyse this region, a Voigt function was employed for deconvolution, enabling curve fitting and identification of the band assignments. Fig. 6 illustrates the results of this process for pulp fibre and cellulose film from colloidal solution, respectively. Consistent with previous studies by Lee *et al.*, hydrogen bonding in cellulose is characterised by the activity of inter- and intrachain hydrogen bonds within the cellulose unit.[34]

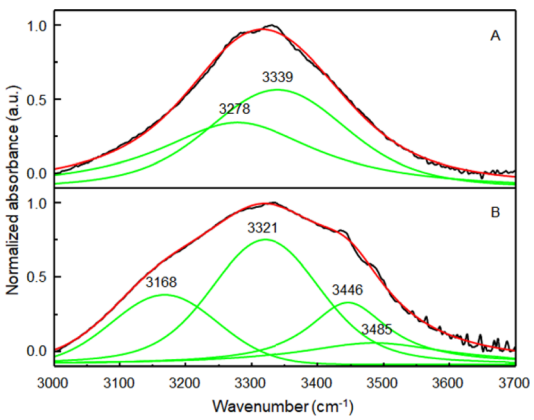

Fig. 6 FT-IR spectra of (A) pulp fibre and (B) cellulose film with Voigt curve fitting in the range of 3000–3700 cm^{-1}.

The deconvolution of the IR spectra suggests two distinct regions: intrachain and coupled hydrogen bonding within the cellulose unit (3270–3410 cm^{-1}) and hydrogen bonding in less-crystalline cellulose or on cellulose surface regions (~3450 cm^{-1}). The prominent peaks in the less-crystalline or surface regions in Fig. 6B imply the occurrence of hydrogen bonding within the low-crystallinity structure forming the cellulose film. Additionally, this finding is consistent with the weak vibrational mode observed at 1435 cm^{-1} (blue dashed line, Fig. 3) in the treated sample. Therefore, the formation of cellulose film should also decrease the cellulose's crystallinity.

To explain the film formation, colloidal cellulose with high water content may undergo particle–particle bonding *via* hornification during the drying process.[48] Hornification reduces the crystallinity of cellulose,[49] thus explaining the low-crystallinity structures observed in both the XRD pattern (Fig. 2) and IR spectra (Fig. 3 and 6). To explore this aspect further, the thermal decomposition profile of the cellulose film was analysed by TGA (ESI, Fig. S4†). A gradual weight loss of approximately 10% at up to 150 °C corresponds to the loss of residual moisture or loosely bound water within the cellulose structure,[50] thus indicating that some water molecules remain within the cellulose film. The TGA results support the concept that cellulose accumulation from small colloidal particles (crystalline and non-crystalline forms) into a larger film occurs when trace amounts of water are present, consistent with the hornification process.[48] Furthermore, the presence of trace water corresponds to the vibrational mode at a wavenumber of 3485 cm^{-1}, indicating hydrogen bonding between hydroxyl groups and interlayer water (Fig. 6B).[51] Overall, by integrating the data from electron microscopy, vibrational spectroscopy, and thermal decomposition profiles, the assembly of colloidal cellulose can be schematically illustrated as a process driven by hornification, as shown in Fig. 7.

3.4. Application with crop protection

To demonstrate the advantages of colloidal cellulose, the material obtained in this study was utilised as a dispersive medium for Cu_2O, a widely used antifungal agent in agriculture.[52] A 1.0% w/v colloidal cellulose solution containing 200 mg L^{-1} Cu_2O was tested for its ability to reduce the growth

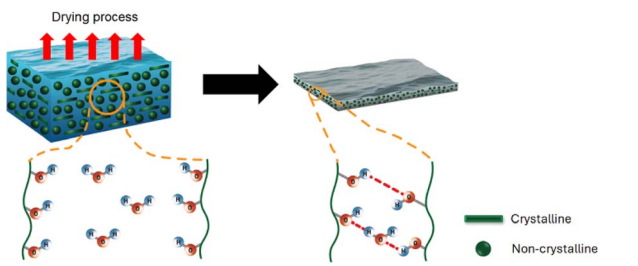

Fig. 7 Schematic representation of the transformation of colloidal cellulose into a film *via* the hornification process, including drying and hydrogen bonding within cellulose units.

Open Access Article. Published on 09 October 2024. Downloaded on 4/26/2026 2:10:51 AM.
This article is licensed under a Creative Commons Attribution-NonCommercial 3.0 Unported Licence.

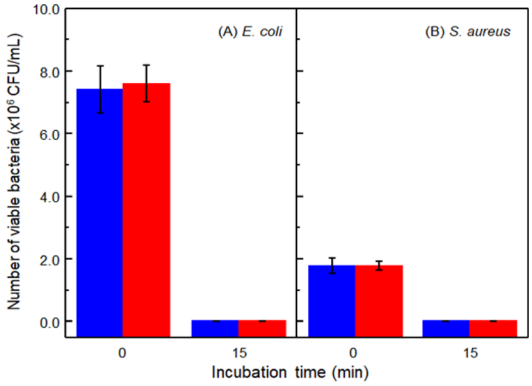

Fig. 8 Plot showing the antimicrobial efficacy of Cu_2O, both in the presence (blue bar) and absence (red bar) of colloidal cellulose, which was assessed by measuring the number of viable bacteria, specifically (A) *E. coli* and (B) *S. aureus*, at 0 and 15 minutes.

of *E. coli* and *S. aureus*, thus measuring the antimicrobial efficacy of Cu_2O. The reduction in bacterial growth was assessed by measuring the number of viable bacteria in colony-forming units (CFU) before and after 15 minutes of treatment with Cu_2O, with and without colloidal cellulose, as shown in Fig. 8. The percentage reduction was calculated using eqn (2).[53]

$$\%\ \text{reduction} = \frac{(B - A)}{B} \times 100 \quad (2)$$

where A and B represent the number of viable bacteria after and before treatment (CFU mL^{-1}), respectively. The results indicated that both Cu_2O alone and Cu_2O with colloidal cellulose reduced the number of viable *E. coli* and *S. aureus* by >99%, with no significant difference in antimicrobial activity recorded between the two treatments (Fig. 8). This suggests that colloidal cellulose does not interfere with the antimicrobial properties of Cu_2O and can therefore be combined with agricultural agents to potentially enhance the contact time and coverage on complex plant surfaces.

4. Conclusions

In this study, we successfully synthesised colloidal cellulose with excellent water dispersibility through the acidic treatment of eucalyptus pulp. The optimised conditions, involving 24 hours of treatment, produced colloidal cellulose with an average particle size of 0.57 ± 0.03 μm, representing the smallest particle size achieved. Following the incubation and drying processes, the crystallinity of the cellulose decreased due to hornification, leading to the formation of a film with adhesive properties on complex plant surfaces. Importantly, the presence of colloidal cellulose did not diminish the efficacy of crop protection agents, as evidenced by consistent antimicrobial efficiency in formulations with and without the colloidal additive. Therefore, colloidal cellulose, with its high compatibility with plant surfaces, holds significant potential as a sustainable coating agent or adjuvant in agricultural protection strategies.

Data availability

The data that support the findings of this study are available on request from the corresponding author. The data are not publicly available due to privacy or ethical restrictions.

Author contributions

A. Phengdaam: writing – review & editing, visualization conceptualization, supervision, and funding acquisition. J. Chaiyosburana: methodology, validation, and investigation. W. Hianchasri: writing – original draft, methodology, validation, and investigation. N. Khupsathianwong: resources and methodology. N. Uthaipan: resources and methodology. S. Ekgasit: writing – review & editing, supervision, and funding acquisition.

Conflicts of interest

The author declares no conflict of interest.

Acknowledgements

This work supposed by Research and Innovation Grant N83A671168 from the National Research Council of Thailand (NRCT). A. Phengdaam would like to thank the Rubber Authority of Thailand (grant number 001/2567) for partially financial support.

References

1 G. Tonoli, E. Teixeira, A. Corrêa, J. Marconcini, L. Caixeta, M. Pereira-da-Silva and L. Mattoso, *Carbohydr. Polym.*, 2012, **89**, 80–88.
2 V. K. Thakur, M. K. Thakur and R. K. Gupta, *Carbohydr. Polym.*, 2013, **97**, 18–25.
3 D. V. H. Thien, D.-N. Lam, H. N. Diem, T. Y. N. Pham, N. Q. Bui, T. N. T. Truc and D.-T. Van-Pham, *Carbohydr. Polym.*, 2022, **288**, 119421.
4 N. A. Zainul Armir, A. Zulkifli, S. Gunaseelan, S. D. Palanivelu, K. M. Salleh, M. H. Che Othman and S. Zakaria, *Polymers*, 2021, **13**, 3586.
5 C. Lang, *The Pulp Invasion–Thailand*, **https://chrislang.org/2002/12/01/the-pulp-invasion-thailand/**, accessed October 07, 2024.
6 M. A. Herrera, A. P. Mathew and K. Oksman, *Cellulose*, 2017, **24**, 3969–3980.
7 M. Hamedi, E. Karabulut, A. Marais, A. Herland, G. Nyström and L. Wågberg, *Angew. Chem., Int. Ed.*, 2013, **52**(46), 12038–12042.
8 S. S. Z. Hindi, *Nanosci. Nanotechnol. Res*, 2017, **4**, 17–24.
9 N. Chandel, K. Jain, A. Jain, T. Raj, A. K. Patel, Y.-H. Yang and S. K. Bhatia, *Ind. Crops Prod.*, 2023, **201**, 116929.
10 A. Blanco, M. C. Monte, C. Campano, A. Balea, N. Merayo and C. Negro, in *Handbook of Nanomaterials for Industrial Applications*, Elsevier, 2018, pp. 74–126.

© 2024 The Author(s). Published by the Royal Society of Chemistry

Open Access Article. Published on 09 October 2024. Downloaded on 4/26/2026 2:10:51 AM.
This article is licensed under a Creative Commons Attribution-NonCommercial 3.0 Unported Licence.

11 A. Gamage, R. Gangahagedara, J. Gamage, N. Jayasinghe, N. Kodikara, P. Suraweera and O. Merah, *Farming Syst.*, 2023, **1**, 100005.
12 M. Ioelovich, *Polymers*, 2021, **13**, 4313.
13 W. Cao, W. Zhang, L. Dong, Z. Ma, J. Xu, X. Gu and Z. Chen, *Exploration*, 2023, **3**, 20220169.
14 M. Zhou, D. Chen, Q. Chen, P. Chen, G. Song and C. Chang, *Adv. Mater.*, 2024, **36**, 2312220.
15 W. D. Jang, J. H. Hwang, H. U. Kim, J. Y. Ryu and S. Y. Lee, *Microb. Biotechnol.*, 2017, **10**, 1181.
16 H. Wang, H. Xie, H. Du, X. Wang, W. Liu, Y. Duan, X. Zhang, L. Sun, X. Zhang and C. Si, *Carbohydr. Polym.*, 2020, **239**, 116233.
17 M. Börjesson, K. Sahlin, D. Bernin and G. Westman, *J. Appl. Polym. Sci.*, 2018, **135**, 45963.
18 T. Ma, X. Hu, S. Lu, R. Cui, J. Zhao, X. Hu and Y. Song, *Int. J. Biol. Macromol.*, 2021, **184**, 405–414.
19 Z. Shang, X. An, F. T. Seta, M. Ma, M. Shen, L. Dai, H. Liu and Y. Ni, *Carbohydr. Polym.*, 2019, **222**, 115037.
20 U. Molin and A. Teder, *Nord. Pulp Pap. Res. J.*, 2002, **17**, 14–19a.
21 U. Molin and G. Daniel, *Holzforschung*, 2004, **58**, 226–232.
22 K. Phuphantrakun, A. Chandrachai and S. Ekgasit, *Trends Sci.*, 2023, **20**, 5496.
23 Q. Zhang, M. Benoit, K. D. O. Vigier, J. Barrault, G. Jégou, M. Philippe and F. Jérôme, *Green Chem.*, 2013, **15**, 963–969.
24 K. Khotmungkhun, W. Chaengsawang, T. Srikhirin, R. P. Poo-arporn, G. Doungchawee and K. Subannajui, *ACS Appl. Nano Mater.*, 2022, **5**, 4462–4472.
25 J. Kong-Win Chang, X. Duret, V. Berberi, H. Zahedi-Niaki and J. M. Lavoie, *Front. Chem.*, 2018, **6**, 117.
26 K. J. Dussan, D. Silva, E. Moraes, P. V. Arruda and M. Felipe, *Chem. Eng. Trans.*, 2014, **38**, 433–438.
27 L. Peltonen and C. Strachan, *Molecules*, 2015, **20**, 22286–22300.
28 I. S. Goldstein, in *Encyclopedia of Forest Sciences*, ed. J. Burley, Elsevier, Oxford, 2004, pp. 1835–1839, DOI: **10.1016/B0-12-145160-7/00042-9**.
29 S. Park, J. O. Baker, M. E. Himmel, P. A. Parilla and D. K. Johnson, *Biotechnol. Biofuels*, 2010, **3**, 10.
30 L. Segal, J. J. Creely, A. Martin Jr and C. Conrad, *Text. Res. J.*, 1959, **29**, 786–794.
31 H. Wang and J. Zhou, *Acta Phys. Pol., A*, 2016, **130**, 886–888.
32 A. W. Pratama, M. Mahardika, N. Widiastuti, B. Piluharto, R. Ilyas, S. Sapuan, D. Amelia and A. Firmanda, *Case Stud. Chem. Environ. Eng.*, 2024, **9**, 100743.
33 T. Seki, K.-Y. Chiang, C.-C. Yu, X. Yu, M. Okuno, J. Hunger, Y. Nagata and M. Bonn, *J. Phys. Chem. Lett.*, 2020, **11**, 8459–8469.
34 C. M. Lee, J. D. Kubicki, B. Fan, L. Zhong, M. C. Jarvis and S. H. Kim, *J. Phys. Chem. B*, 2015, **119**, 15138–15149.
35 Y. Wang, Y. Wang, J. Cheng, H. Chen, J. Xu, Z. Liu, Q. Shi and C. Zhang, *Crystals*, 2021, **11**, 1440.
36 H. J. Ensikat, P. Ditsche-Kuru, C. Neinhuis and W. Barthlott, *Beilstein J. Nanotechnol.*, 2011, **2**, 152–161.
37 M. Alves, D. Andrade, L. Mesquita, L. Barreira, J. Manhique, S. Echart, M.-F. Barreiro and F. Mofreita, *AIP Conf. Proc.*, 2023, **2928**, 080030.
38 T. Hata, *J. Adhes.*, 2006, **4**, 161–170.
39 S. Ebnesajjad, in *Handbook of Adhesives and Surface Preparation*, ed. S. Ebnesajjad, William Andrew Publishing, Oxford, 2011, pp. 3–13, DOI: **10.1016/b978-1-4377-4461-3.10001-x**.
40 A. Tsikrikis, T. Papaliangas and V. Marinos, *Geotech. Geol. Eng.*, 2022, 1–17.
41 H. Wang, X. Shi, Y. Xie, S. Gao, Y. Dai, C. Lai, D. Zhang, C. Wang, Z. Guo and F. Chu, *Cell Rep. Phys. Sci.*, 2023, **4**, 101374.
42 S. Gao, Y. Liu, C. Wang, F. Chu, F. Xu and D. Zhang, *Polymers*, 2020, **12**, 638.
43 B. Kabiri Far and C. Zanotti, *Appl. Sci.*, 2019, **9**, 2556.
44 J. A. von Fraunhofer, *Int. J. Dent.*, 2012, **2012**, 951324.
45 M. C. Jarvis, *Cellulose*, 2023, **30**, 667–687.
46 C. R. Frihart, *Handbook of Wood Chemistry and Wood Composites*, 2005, pp. 255–313.
47 D. Zhao, Y. Deng, D. Han, L. Tan, Y. Ding, Z. Zhou, H. Xu and Y. Guo, *Carbohydr. Polym.*, 2019, **204**, 247–254.
48 L. Salmén and J. S. Stevanic, *Cellulose*, 2018, **25**, 6333–6344.
49 J. E. M. Ballesteros, S. F. Santos, G. Mármol, H. Savastano and J. Fiorelli, *Constr. Build. Mater.*, 2015, **100**, 83–90.
50 S. Kumar, L. Prasad, P. P. Bijlwan and A. Yadav, *Biomass Convers. Biorefin.*, 2024, **14**, 12673–12698.
51 S. Wang and Y. Zhang, *Colloids Surf., A*, 2024, **701**, 134951.
52 D. Rusjan, in *Fungicides for Plant and Animal Diseases*, IntechOpen, 2012.
53 K. Jung Woo, C. Koo Hye, W. Kim Ki, S. Shin, H. Kim So and H. Park Yong, *Appl. Environ. Microbiol.*, 2008, **74**, 2171–2178.